SYNTHESIS REPORT

For publication

CONTRACT N°: BRE2-CT92-0150

PROJECT N°: 5106

TITLE: *DESIGN OF ADVANCED MATERIALS FOR COLD FORGING TOOLS BY MACRO- AND MICROMECHANICAL MODELLING*

COORDINATOR: Prof. Dr. Ing. D. Weichert.

PARTNERS:

1. Institute för Metallforskning
   S -11428 Stockholm

2. Laboratoire de Mécanique de Line,
   CNRS URA 1441,
   F -59655 Villeneuve d'Ascq Cedex

3. Institut für Werkstoffe,
   Ruhr Universität Bochum,
   D -44780 Bochum

STARTING DATE: 1.1.1993 **DURATION:** 36 months

PROJECT FUNDED BY THE EUROPEAN COMMUNITY UNDER THE BRITE-EURAM PROGRAMME

A New Material for Cold Forging Tools

H. Berns*, A. Melander#, D. Weichert$,
N. Asnafi#, C. Broeckmann*, A. Groß-Weege$

* Institut fur Werkstoffe, Ruhr-Universität Boc hum, Germany
# Institute for Metallforskning, Stockholm, Sweden
$ Laboratoire de Mécanique de Line, France

Abstract

A new tool material for cold forging applications was developed using numerical simulation techniques (FEM) for the design and a powder metallurgical route (HIP) for the production. The basic idea was to find an optimized microstructure of the two phase material by simulating different distributions of hard particles within the metal matrix. On the micro-scale, loading was applied by a field of deformations which was obtained by a microscopical simualtion of a particular cold forming process in bolt making. A new double dispersion microstructure was found to show the best resistance against crack propagation. Specimens were produced by hot isostatic pressing. Afterwards the new material was tested in the laboratory. Wear resistance and bending strength of the double dispersive material are comparable to a standard dispersion material with the same volume fraction of particles, but fracture toughness is increased by about 30%. Testing the new material in bolt making showed that the life time of the tool is increased by a factor of 8.

1. Introduction

Tools in cold forging applications are often subjected to a combination of abrasive wear and mechanical stresses due to the high forces which occur in metal forming processes. Thus, materials used. for these tools must have both high wear resistance and high strength and fracture toughness. As an example for a cold forging process we focus on the heading operation of high-strength bolts used in the automotive industry. Conventional HSS is a typical tool material for die inserts. High wear resistance and high strength are achieved by using these steels in the hardness range of 56-58 HRC. But even at this low hardness level, the fracture toughness K_{Ic} is poor and the life time of the tool is limited by cracks.

The aim of this paper is to present a method for development of optimized materials. This method is based on the numerical simulation of both the microscopical stress field in the tool and the microscopical stress field in the in homogeneous material. In a first step, the state of stress in the tool during the forming process was calculated. Thereby the **most** critical area in the die was identified as the region with the highest equivalent and principal stresses. In a second step the critical area was model led on a microscopical scale. For this simulation the deformation field found by the microscopical simulation was used as a boundary condit on. A two phase calculation was carried out, assigning the- particles and the metal matrix different mechanical properties. Taking into account particle cracking and damage of the matrix, the distribution of particles was optimized with respect to high resistance against crack propagation. In a third step, a tool material with an optimized microstructure was

produced along a powder metallurgical route. Finally the new material was tested in the laboratory and in the shop. In the following, the results obtained in all these three steps **of** the applied method are described.

2. Tool **Stresses**

Manufacturing of fasteners was selected as an appropriate cold forging operation, in which the tool stresses can become critical. Fig. 2.1 displays the selected forging sequence and component geometry, which are identical or very similar to the sequence and geometry of screws from commercial production. As exhibited in Fig. 2.1, the selected fastener was formed in three steps. In the first step, the shank was extruded. In the second step, preheating was conducted, while in the third step, the fastener obtained its final shape. The extrusion of the shank, Fig. 2.1, was not included in the theoretical and experimental analysis. In other words, the tool stresses emerging from preheating and final heading, Fig. **2.1,** were at the focus in this study. Merely some of the results obtained in this investigation are accounted for here. Those interested in the entire outcome of this study are referred to [1 ,2].

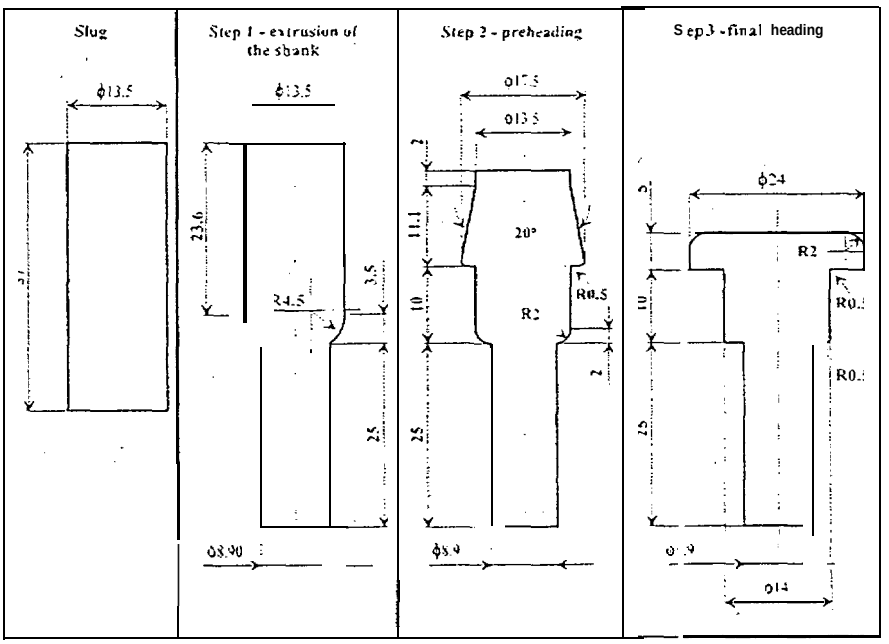

Fig. 2.1. Forging sequence: the initial, intermediate and final shape of the component.

2.1 **Finite element simulation**

A two dimensional (axisymmetrical) finite element sirr ulation, utilizing the code ABAQUS, was carried out. The simulation consisted of three steps - (1) shrink-fitting of the stress ring over the die insert and lower die, (2) preheating & (3) final heading. See Fig. 2,2. The interference fit between the stress ring a **nd the die insert was** 0.2%, **Fig. 2.2,** The workpiece and the die insert were modeled as elasto-plastic isotropic hardening materials. The stress ring and lower die were modeled as elastic bodies. The punches were assumed to be rigid. Table 2.1 gives some of the mechanical" and physical properties of the materials utilized in the finite element simulation. In, this table, σ_y = yield strength, E = modulus of elasticity, v :: Poisson' s ratio, and α = coefficient of thermal expansion.

Material	**Used as**	σ_y **(M Pa)**	**E (MPa)**	v	α ("C-')	**Hardn. (HRC)**
DIN37Cr4 [1]	Workpiece mat.	***400***	***205000***	***0.30***		
ASP2030 [2]	Die insert mat.	2644	241300	C.30		***6 2***
H13 (AISI) [3]	Stress ring mat.		194000	C.30	$12.6\text{-}10^{-6}$	58
G 5 (cemented carbide) [4]	Lower die mat.		461000	C.24		

Tab 2.1 Some mechanical and physical properties of the used materials. 1) The values are extracted from [3], 2) E and σ_y were measured by compression tests. See also [4]. 3) The values come from [5]. 4) The values are extracted from [6].

2.2 **Experimental Procedure**

The die insert was manufactured in ASP2030 and the stress ring in H13 (AISI), Table 2.1. Channels were machined **in** the die insert 'and the stress ring to obtain space for strain gages and lead wires. The stress ring was heated and shrink-fitted over the inner dies. One strain gage was bonded on the die insert and one on the stress ring. To register the forging load, a 1 MN load cell was used. An extensiometer was, furthermore, used to register the position of the punch (st 'eke) during the cold forging. A PC-based system was used to register the signals from the load cell and the strain gages. The forgings **were** conducted in a 2.5 MN hydraulic press.

2 . 3 **R e s u l t s**

2.3.1 **Finite element simulation**

The mesh deformation at the end of the final heading is shown in Fig. 2.2. The most heavily deformed area in the tool arrangement is the zone at the die insert profile radius. This zone is so intensely loaded that plasticity s initiated during the last 0.2 mm of the punch stroke in final heading. A possible cause of tool failure might be that

the shear stresses at the die insert profile radius become critical. The distribution of the shear stress, S12, in the zone around the die insert profile radius is, therefore, depicted in Fig. 2.3. There are, as exhibited in Fig. 2.3, two stress zones. (Stress values are given in the legend are in MPa). In the first zone, which is located near the **top** surface of the die insert, the shear stresses are positive, the maximum level being 2030 MPa. In the second zone, which is situated close to the die insert bore wall, the shear stresses are negative, the minimum. level being -9C5 MPa.

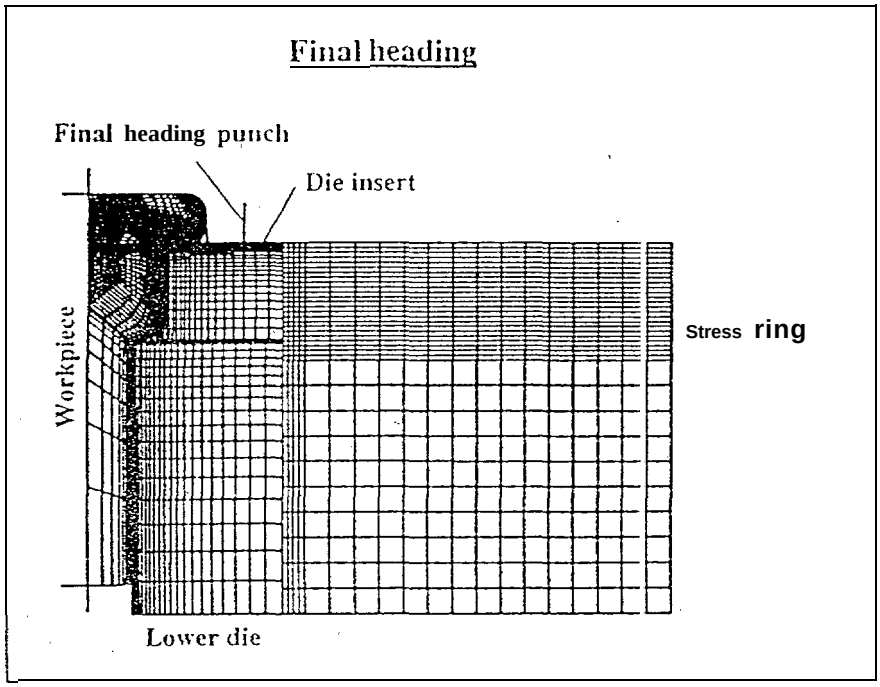

Fig. 2.2 Mesh deformation: cold forging of the final heat.

Considering the (workpiece) material flow at the die insert profile radius, the shear stress distribution in this zone seems. to be plausible. That is since the work material flows both downwards and radially with a neutral zone between these two flows. Chipping at the top inner edge of the die, *i.* e. at the die insert profile radius, is, in practical screw-making, one of the main reasons why die inserts are discarded. The obtained simulation results, Fig. 2.3, correspond, in other - words, well to the circumstances experienced by practitioners. That is provided that the shear stresses are controlling the tool failure.

2.3.2 **Experimental analysis**

Fig. 2.4 displays the heading force as function of the punch stroke during both preheating and final heading. Both finite' element and experimental values are plotted in this figure. Comparing the theoretical values with the experimental at 2, 6 and 8 mm in punch stroke, a difference 'in magnitude is observed at the beginning of each step, Fig. 2.4. The experimentally obtained values exhibit, though, a good correlation to those attained theoretically, particularly at the end of p-eheading and final heading, Fig. 2.4. 20 fasteners were cold-forged with the sequence shown in Fig. 2,1. No cracking could be observed in the die insert. Forgings were also conducted at Bulten Automotive AB. In these forgings, the same die insert as hat used **in** this investigation was tested. The height of the upper head was, though, 2.5 mm (the height of the upper ,

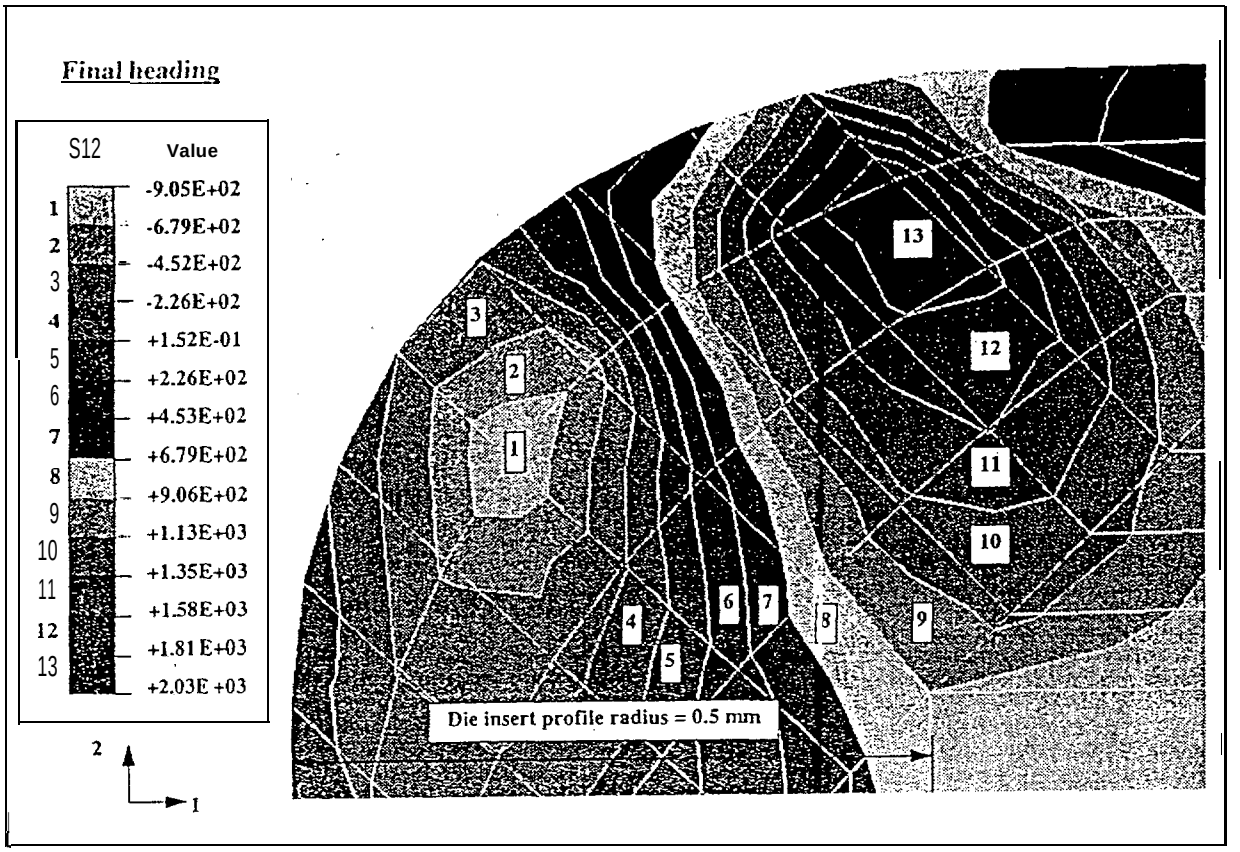

Fig. 2.3 Distribution of the shear stress, S12 , at the die insert profile radius and at the end of forging. The stresses shown in the legend are in MPa

head was 5 mm in our case, Fig. 2.1). In addition to this lower upper head height, a hole was pierced in the upper head, [7]. The forgings conducted at Bulten automotive AB were, in other words, "tougher" than those conducted in this investigation. After producing 9080 parts at Bulten automotive AB the die insert bore became conical and the **die** insert cracked at two sites [7].

All this information together with the results obtained at Bulten Automotive AB indicate that high cycle fatigue, and not monotonic rupture, is the main cause of" fracture in practice. The conducted finite element simulations can, therefore, be used to find the strain and/or stress range within which the fatigue properties should be studied.

2.4 **Conclusions**

The following conclusions are due:

The developed method for finite element simulation of the mechanical state in cold forging tools can be used as a robust device in predict on of strains an'd stresses in tools and in tool design in manufacturing of fasteners.

The heading force and the radial and circumferential stra ns obtained by finite element simulation exhibit a close agreement with those found experimentally.

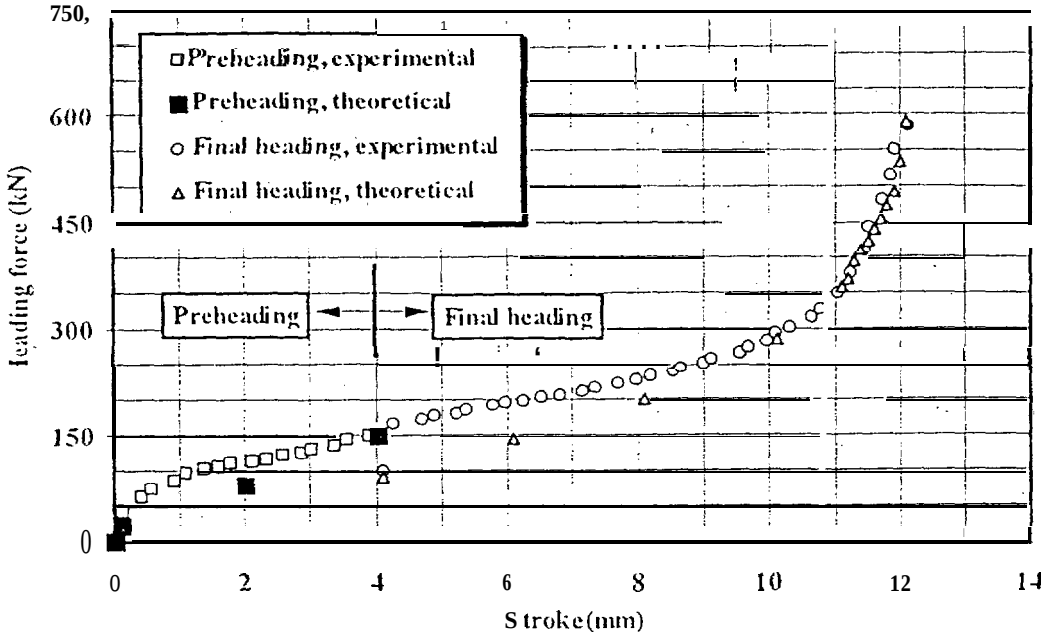

Fig. *2.4* Theoretically (FEM) and experimentally obtained heading force as function of the punch stroke. Both the preheating and the final heading forces are plotted.

Although 20 fasteners were cold-forged in this investigation, the die insert did not fracture at the profile radius. A similar die insert could under "tougher" production conditions withstand 9080 part before cracking. This implies that high cycle **fatigue,** and not monotonic rupture, is the main cause of tool failure in practice. The conducted finite element simulation can, therefore, be used to find the strain and/or stress range (-s) within which the fatigue properties could be studied.

3. Micromechanical **optimization of the** microstructure

3.1 Model description

Geometrical model

The main objective of these studies is to model specific microscale arrangements which are characteristic **for** the here investigated class of materials where **one** phase (HP) is distributed discretely in a continuous second phase (MM) (so-called matrix- - inclusion topologies). The geometrical parameters describing this type of microstructure, are the volume content, size, shape and arrangements of HP. Within the definition of a representative volume element (R.V. E,), the microstructure may be effectively covered by periodically arranged unit cells Increasing their degree of randomness, unit cells describe more realistic microstructure but do cost more computational effort. Unit cells with a lower level of randomness (perfect periodic, clustered arrangements) have e.g. been employed to inv estigate arrangement effects on the micro- and macroscale response of unidirectional continuously reinforced metal matrix composites (MMCs) [8,9].

However, they **seem** not to be useful for damage simulation, since microcracking would occur throughout the structure at the same time step [10,1 1]. In order to

investigate the evolution of damage due to particle cracking, a unit cell with 16 randomly distributed HP is used in the present study (called in the following Dispersion). The shape of the HP are assumed to 'be cylinders (for plane strain) or circular discs (for plane stress). In each case, all HP have the same shape.

Beside the dispersion, arrangements are considered, where HP have been concentrated within one region with high volume content (the colony), the other region with no HP-presence. The colonies, are localized within cylinders (or circular sheets), these in turn distributed perfectly within a hexagonal arrangement (called in the following Double Dispersion), the region around the above described cylinders (called in the following Net) and bands (called in the following Band). Figure 3.1 illustrates schematically the unit cells of the different arrangements

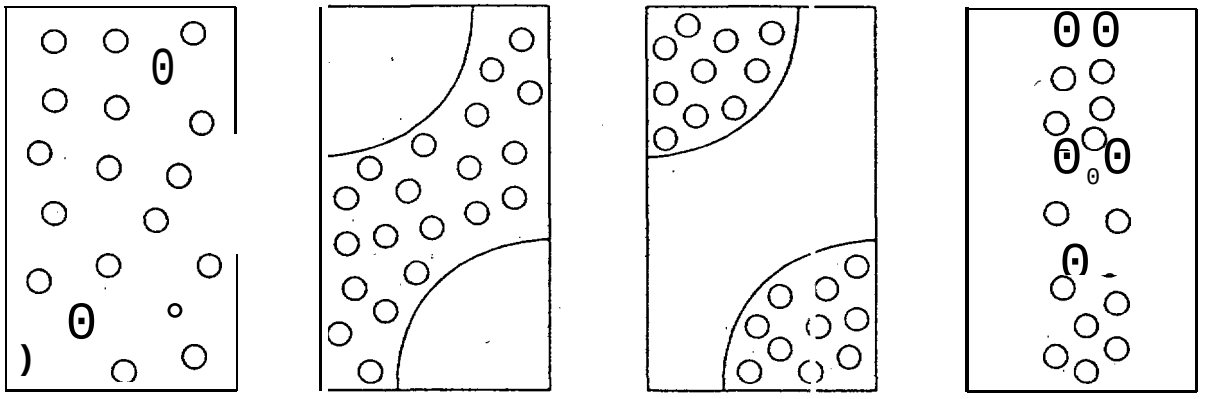

Fig. 3.1 Different classes of matrix-inclusion topologies inherent in the unit cells

The boundary conditions are taken such that symmetry is prescribed over all edges of the cell. The number of HP (N_{HP}=16) and the respective volume fraction (ξ_{HP}=15%) are equal in all unit cells. **The** considered arrangements are representative to a certain extent for the microstructural arrangement of the investigated materials: Conventional materials: The banded structure shall describe' the microstructure after warm forging, the net-like structure that in the as-cast condition. PM-HIP materials: The dispersion is typical for materials manufactured by powder metallurgy and hot-isostatic pressing. In particular the chosen reference material ASP30 and ASP60 show such a microscale topology. The double dispersion may be obtained using two different powder types.

Material Model

Different components inherent in the material are characterized by assigning them different constitutive relations. Based on experimental findings the "following constitutive model has been proven useful to describe the mechanical behaviour of the individual components.

1-The hard phases (HP) represent different carbides of the reference material ASP30 like MC and M_6C carbides. Since it is rather difficult to determine their elastic properties; they were replaced by one equivalent HP. Due to experimental evidence it is assumed that HP will fail by cleavage prior to deform plastically. Isotropic elasticity is described by Hooke's law. Cleavage of HP is suggestec, if the normal stress within the HP reaches a critical value (fracture strength). Keeping the complexity of

programming reasonable, possible crack paths within the HP are predefine. If the criterion for one possible crack path is satisfied, additional nodes are introduced to automatically simulate *microcracking* [12].

2-The metal matrix (MM) is modelled isotropic, elastic-plastic using von Mises plasticity and isotropic hardening. A damage indicator based on Rice&Tracey's [13] void growth model is used to predict initiation of damage in the matrix. The damage indicator is defined following [14] as

$$D; = \int_0^{\varepsilon_v^p} \frac{e^{(1,5\zeta)}}{1,65\varepsilon_0} d\varepsilon_v^p \qquad (3.1)$$

where $\zeta=\sigma_H/\sigma_v$ is the stress triaxiality and σ_H, σ_v and ε_p^v are the hydrostatic stress, effective (v. Mises) stress and the--equivalent plastic strain respectively. The uniaxial failure strain ε_0 is the only adjustable material parameter.

3-The interface is modelled as an orthotropic thin layer. Initially the interface possesses the isotropic elastic-plastic characteristics of the matrix. Interracial failure is assumed to occur' under pure mode I (tensile failure) and pure mode II (shear failure) when the radial and shear interracial stresses reach a critical value, respectively. If the failure criterion is satisfied within one interface element, the orthotropic elastic moduli expressed in the principal axis of orthotropy (normal to the interface) and the respective stress components are modified such that the conditions on the created free (or sliding) surfaces are satisfied.

Material parameters

All material parameters of the components used in the talc ulations are listed together below.

	E (GPa)	ν	$0_{\%}$ (MPa)	σ_{Ic} (MPa)	σ_{IIc} (MPa)	ε_0
metal matrix	2 1 0 '	0,3	1550			0.02
hard phase	400	0 , 3		1 6 0 0		
interface	210	0,3		1600	1600	

Tab. 3.1 Mechanical properties of the components

The flow curve of the metal matrix was determined by a combined experimental and numerical procedure [15] and is entered to the model as a piece-wise hardening curve. The corresponding stress-strain couples can be found in [15]. The Young's modulus of the HP was predicted by a semi-analytically based mean-phase estimate [16].

3.2 Results-Microscopic Response

Progressive carbide fracture

The load is applied incrementally and displacement controlled. Load direction is the vertical axis. The macroscopic load is strain driven and com puted through the imposed displacement values u_y and the length l of the modelled volume:

$$\bar{E}_{yy} = \frac{u_y}{l} \tag{3.2}$$

Damage evolution in this material is simulated by activating the local damage criterion of particle fracture and by quasi-static proportional loading applying successively small load steps. In the experiments particle cracking was observed to be the dominant damage mecanism; therefore the effects of debonding and matrix damage are excluded in this analysis for the first. The following figures aim to illustrate how damage is initiated and evolves by progressive carbide fracture in the different microstructure (exemplarily for the banded (Fig. 3.2; a,b load parallel to the bands, c,d load perpendicular to the bands), double dispersion (Fig. 3.3a, b) and net-like (Fig. 3.3c,d) structure), The results show the maximum principal stress distribution. All values are given in MPa.

Stage up to initial damage: Before the onset of damage stress concentrations arise mainly within the particle. This may be attributed to the occurrence of interracial shear stresses which give an important contribution to the trans mission of the load over the particle. The development of interracial stresses' itself is dependent on how the deformation of the matrix is constrained by the stiffer par icles. This may be strongly influenced when HP are interacting with each other. HP-Interaction shall be understood as an intersection of local disturbed stress fields around individual HP. This interaction behaviour might have a shielding or an amplification character depending on the orientation of adjacent particles to the principal load directic n. The stress concentration within the particle is increasing when the trajectory of adjacent HP is in line with the principal load path and decreasing when it is perpendicular to that.

This effect becomes visible when studying the situation in the banded structure, If the load is applied parallel to the band (Fig. 3.3a), the stress values within the HP and in the matrix are different of order 1,375. When the load is applied perpendicular to it (Fig. 3.3c), the ratio of the stresses in both regions is abo ut 1,135. Increasing the HP-content in these bands would decrease the HP-spacing. As a consequence these results tend to approach the lower and upper bounds in elasticity (bounds by Voigt and Reuss [15]) for infinite aligned HP.

This idea, that HP belonging to one row act as *a* single aligned HP, is furthermore supported when studying initial damage in the double dispersion (Fig. 3.3a, b) and particularly in the net-like structure (Fig. 3.3c,d).

In the latter arrangement damage is initiated in those particles located at the mid-length of one row in load direction (Fig. 3.3c, Fig. 3,4). Indeed, it is known from former studies [l O] 'that single aligned HP do not break randomly along their length; instead fracturing is more likely in the vicinity of the centre of HP

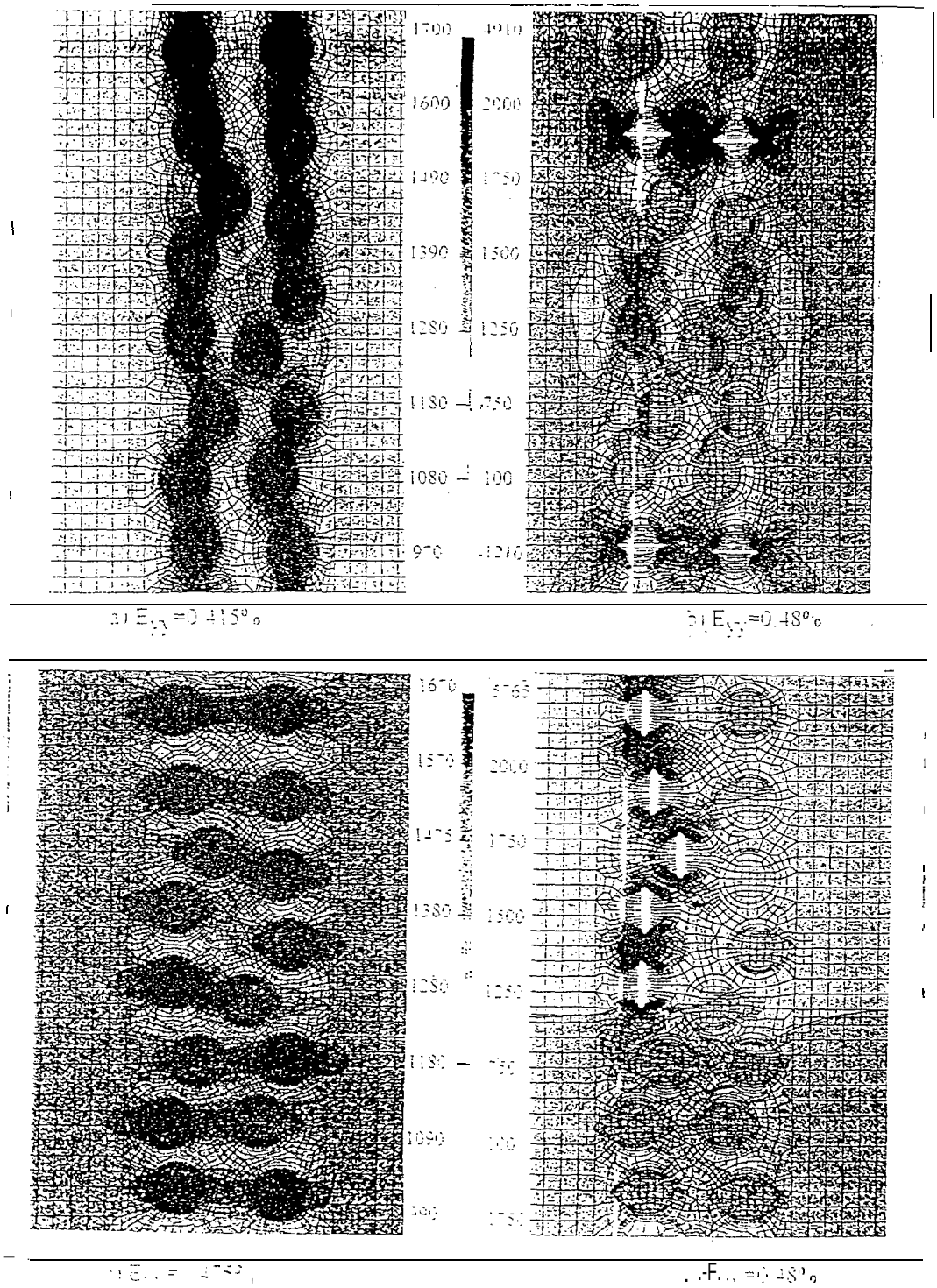

Fig. 3.2 Maximum principal stresses o, [MPA] in the banded arrangement (a-b) load in vertical axis; (c-d) load in horizontal axis

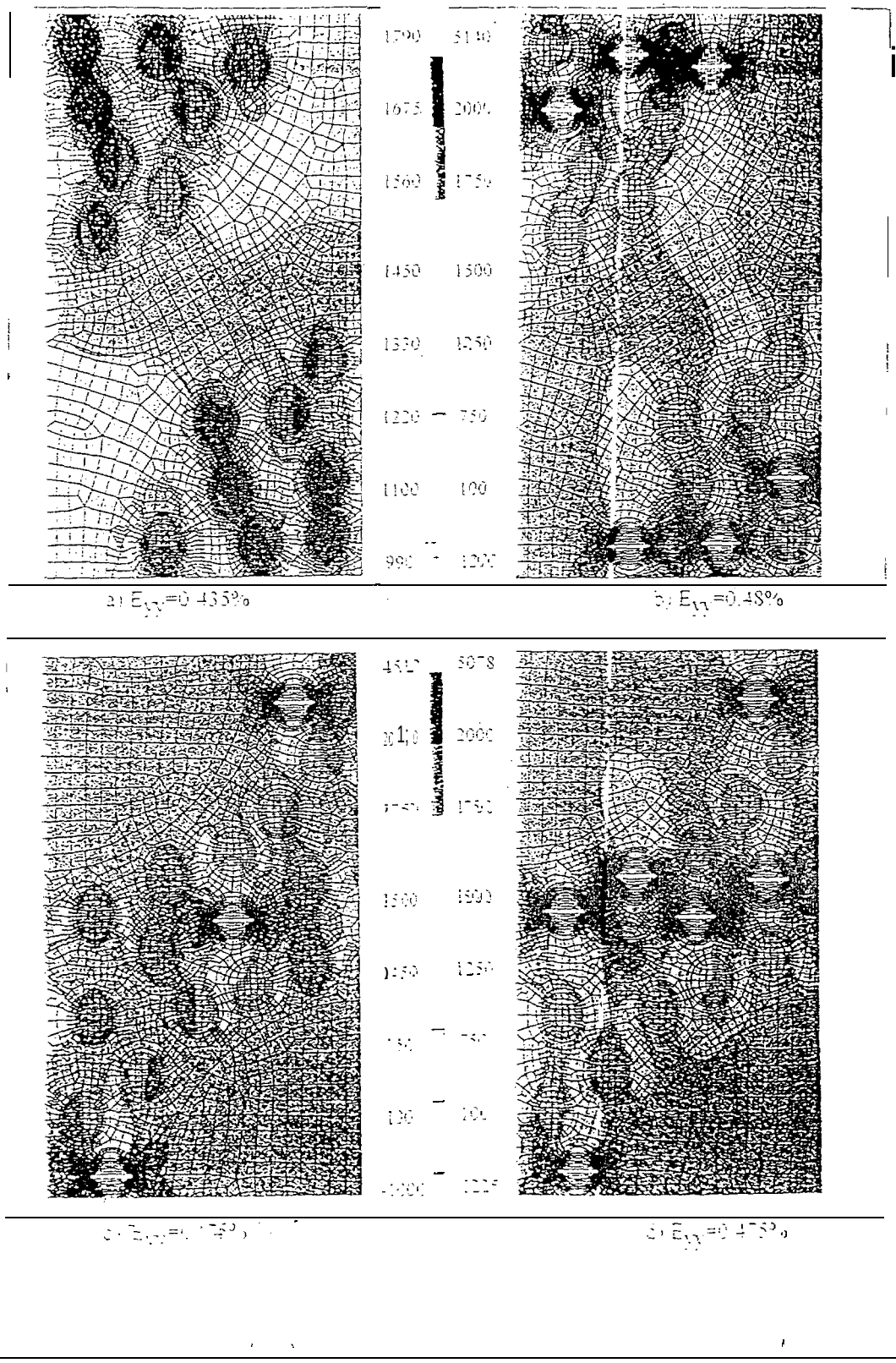

Fig. 3.3 Maximum principal stresses σ_1[MPA] In the (a-b) double dispersion; (c-d) net-like arrangement

Subsequent occurrence of damage Subsequent failure of HP due to fracture is strongly related to their orientation to previously developed microcracks. Mostly, stress redistribution due to cracking of a HP leads to simultaneous microcracking of adjacent HP (in direction of the microcrack) without increasing the external load. In particular in the band direction, first HP-fracture leads to a chain reaction where subsequently the neighboring particle is cracked.

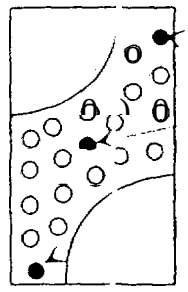

middle of one row

Fig. 3.4 Damage initiation in the net-like structure

Since all microcracks ly within a trajectory perpendicu ar to the load direction, final - material failure is expected by fracture of the matrix ligaments under mode 1. The failure in the matrix ligaments is believed to be dependent on the orientation and spacing of neighboring microcracks and the ductility of the matrix, In particular, the continuity of regions with high HP-content seems to play an important role for the whole deteriorisation process. Accordingly the double dispersion seems 'to be most favorable since the large "matrix net" acts as an important obstacle for microcracks of different clusters to link together.

Competition between particle **cracking** and interracial **failure:**

The competition between both damage mechanisms is investigated exemplarily for the dispersion (Fig. 3.5). In addition to particle cracking the failure criterion of interfacial failure under pure mode I was activated and assumed to be equal to the fracture strength of the particle (σ_{ic}=1600 MPa). Figure 3,5a an d b show the distribution of the equivalent plastic strain and of the damage indicator D_i, respectively.

The first microcrack develops at the interface of the second HP from the left side (Fig. 3.5) extending rather quickly up to a stabilization point where the upper half of the particle is totally debonded and the lower half is shielded by the deflection of the load. As a result, the load is carried by the *neighboring* metal matrix which leads to stress concentration in nearby particles. Here, the orientation between neighboring particles strongly influences the sites of maximum stress values and determines therefore the mode of failure (on the left side particle cracking, on the right side interracial failure). Sudden occurrence of HP-cleavage gives rise to considerable tensile radial stresses at the front of the crack tip which may trigger interracial debonding. This effect could be reproduced in the simulations (Fig. 3.5) and was equally observed in experiments.

Generally the release of energy by microcracking is absorbed by the MM and results in plastic deformation. Some regions show plastic deformation before the onset of damage. However, plastic strains are more elevated in front of the crack tips (up to 13%). **The** crossing of these local plastic fields leads to plastic bands connecting the individual microcracks (Fig. .3.5a):

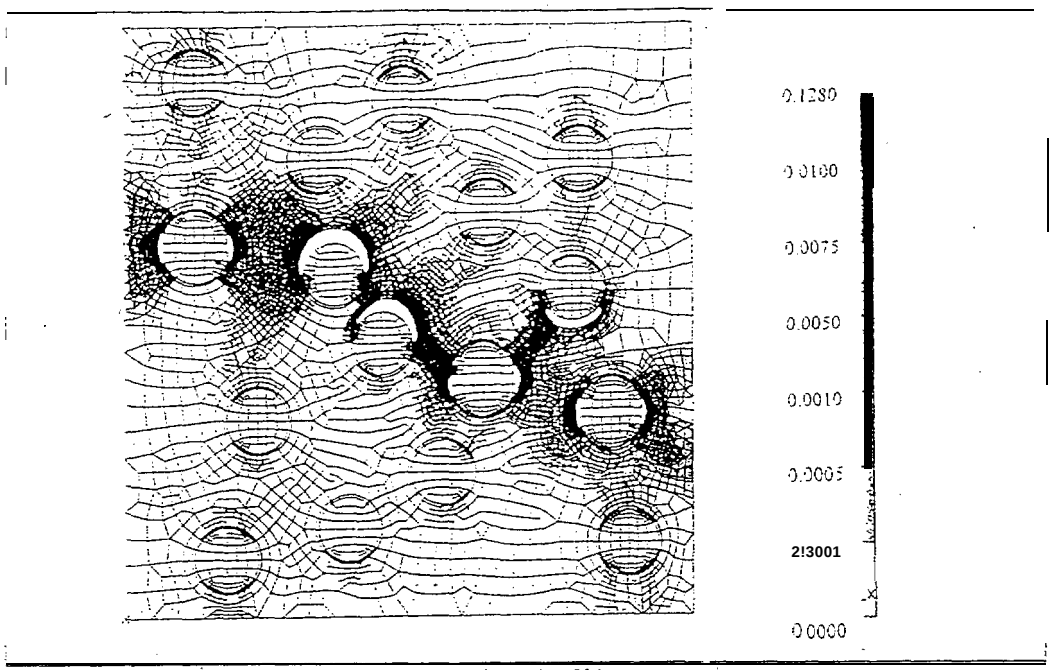

a) E_{yy}=0.45%

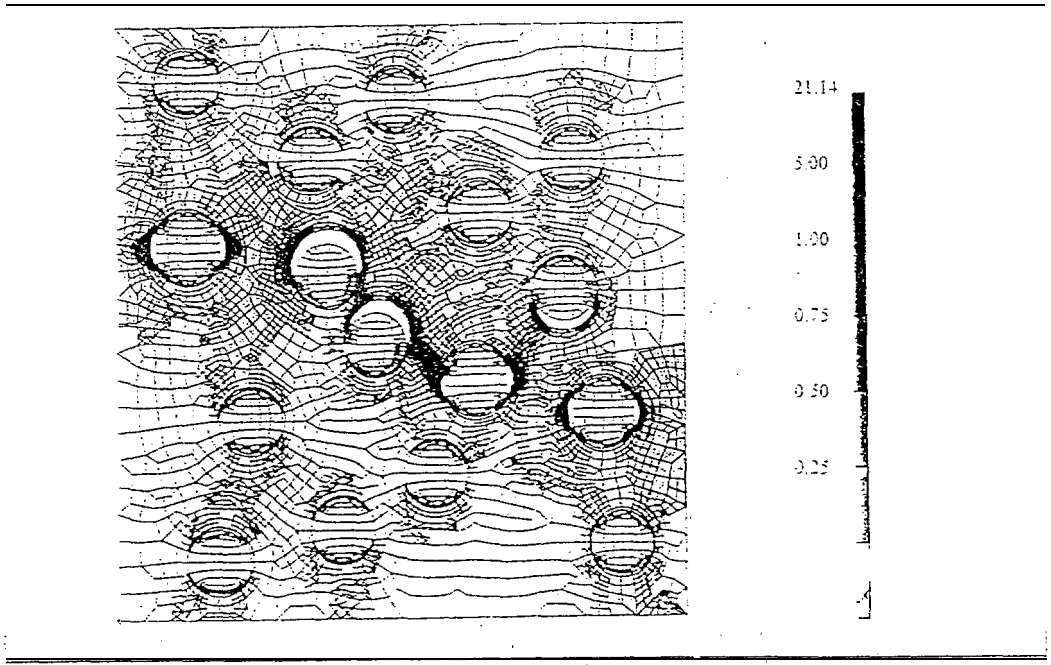

b) E_{yy}=0.45%

Fig. 3.5 Selected damage indicators in the dispersion, (a) Effective plastic strain ε_p^v, (b) Rice&Tracey (for D_i see eq. 3.1) '

In order to-predict the crack path in the matrix the damage indicator presented above **is** also plotted. The damage indicator gets its significiance when assuming a critical limit within the range of values where beyond this value matrix damage is considered. With respect to this definition the predicted crack path seems to be physically reasonable, since one expects ultimate failure by linking together all microcracks. As a result, it is believed that the triaxiality in a plastic field controls crack propagation in the matrix.

4. New double dispersion material

Under tribological as well as mechanical loading a dispersion of hard phases HP shows advantages over a net-like distribution. In grooving wear, hard phases offer best protection if their size is about equal to the groove width. A. a given HP volume the HP spacing increases with HP size, which has a beneficial effect on the fracture toughness. Coarse hard phases, however, impair fracture strength (Fig. 4.1).

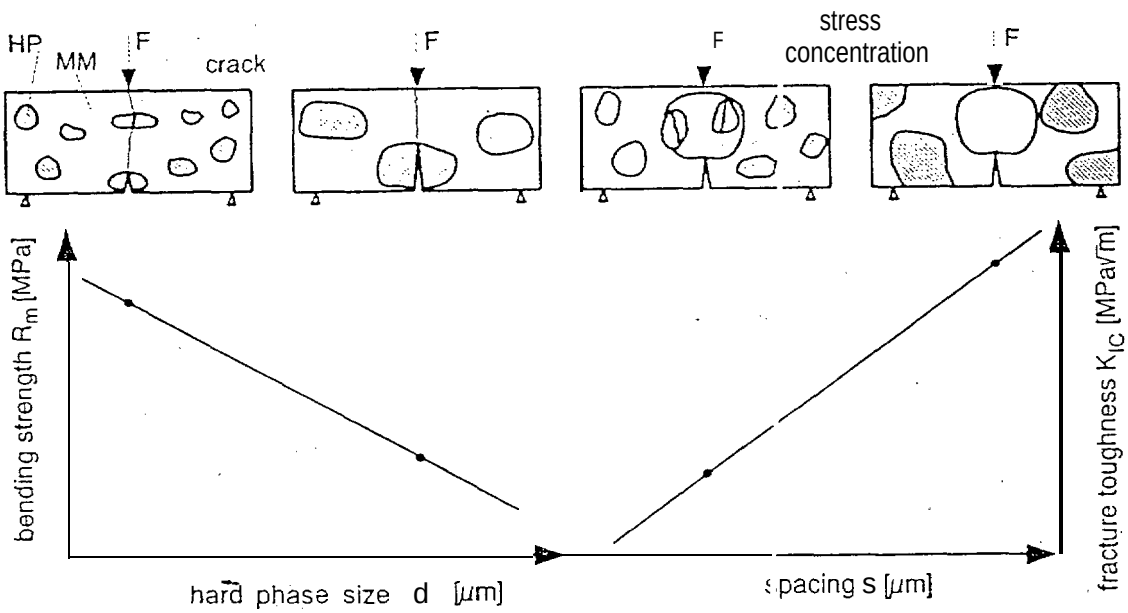

Fig. 4.1 Influence of hard phase size and spacing on strength R_m and fracture toughness K_{Ic}

These results ied to the proposal to replace the coarse hard phases dispersed in a metal matrix MM by a dense dispersion of small hard phases. In other words a homogeneous dispersion of fine hard phases is transformed into clusters of HP. This microstructure is called a double dispersion. As compared to coarse HP the clusters promise a higher fracture strength'. The carbide-free areas between the clusters are meant to increase the fracture toughness.

4.1 Manufacturing

To realize this double dispersion microstructure gas atomized powders **of** spherical shape are used [17], The carbide-rich clusters are made up by a high-carbon high-speed steel powder A with ≈30 vol.-% of fine, dispersed carbides. The ductile areas *B* consist of a hot-work tool steel powder (*B*1) or a low-carbon high-speed steel (62)

(Table 4.1). A mixture of 55 % of powder A and 45 o\o of **powder** *B* **leads to an overall HP** content of ≈ 16.5 % which is equivalent to a PM high-speed steel (PMS) with a homogeneous dispersion of fine HP. The powder grains *A* are dispersed in *B* if they are much larger in size. This is shown in Fig. 4.2 which relates the microstructure after hot compacting to the size ratio and volume ratio of the powders in the mix. **This figure stems from numerous empirical results, as a mathematical** solution is not yet available. At the volume ratio mentioned, an average size ratio of 5 was chosen.

	chemical composition [weight-%]						
	C	Cr	W	Mo	V	Co	others
powder B 1	***0.4***	***5***		***1.4***	1		**1 Si, 0.4Mn**
powder B 2	***0.7***	***4***	***3***	***3***	1		1 Nb
powder A	2.3	4.2	6.5	7	6.5	**10.5**	
PMS	1.3	4.2	6.4	5	3.1	8.5	
PMS A	as powder A						
M 3 class 1	***0.9***	***4***	***6***	5	2		

Tab. 4.1 Chemical composition of steel powder and reference materials

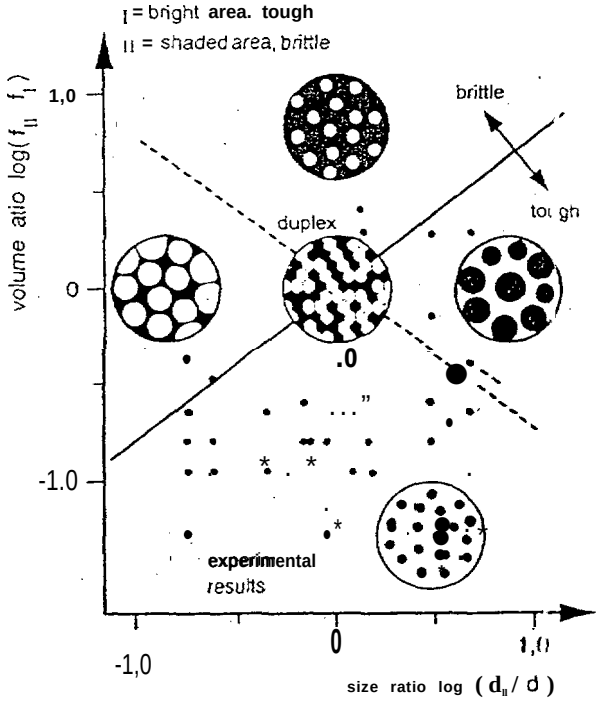

Fig. 4.2 Influence of powder grain size and content of two spherical powders on the PM microstructure

The powder mix was filled into cans which were evacuated, sealed, and hot-isostatically pressed (HIP) at a temperature of 1090 'C under a pressure of 140 MPa. After annealing, the samples were taken, which after hardening and tempering revealed the properties of tables 4.2 and 4.3. The resulting microstructure is shown in fig. 4,3. As the carbon activity in powder *A* is similar to that in powder *B* the interdiffusion of carbon is apparently small. As to the wear resistance, in a pin-on-disk test against abrasive flint paper the double dispersion materials *AB1* and *AB2* are about equal to the reference steel PMS. Looking at the mechanical properties given in table 4.3 the most striking difference between single and double dispersion material is the much higher fracture toughness of the latter.

material	carbide content [vol.-%]			hardness			
				HV *0.05*			*HV50*
	region A (~1µm)	region B (<<1pm)	overall	region A	region B		
AB1	15.0	2.0	17.0	997	817		878
AB2	14.2	2.4	16.6	955	840		889
PMS	16.4		16.4			930	900
PMS A	30,0		30.0			10.30	997

Tab. 4.2 Carbide content and micro hardness of PM materials after HIP and heat - treatment. ABI and AB2 are double dispersion materials of 60 % powder A and 40 % powder B1 and B2. respectively.

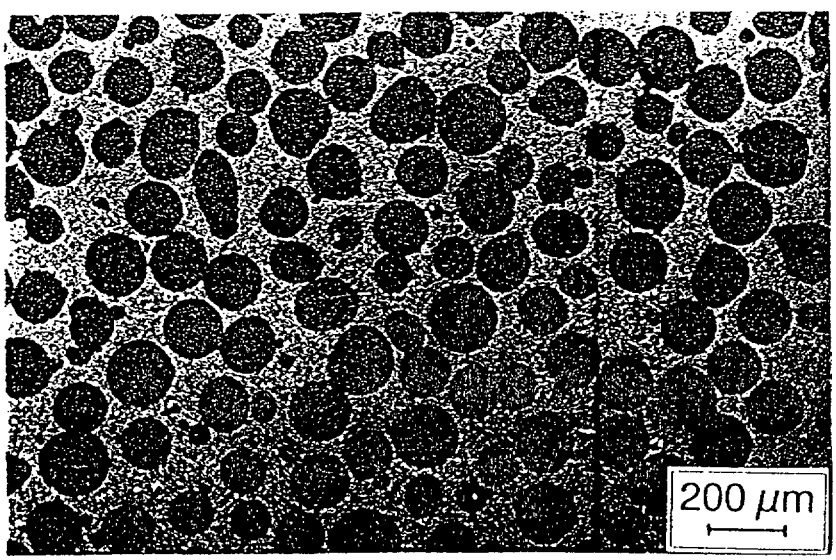

Fig. 4.3 Microstructure of the double dispersion material AB1 (photograph taken by S E M j

Material	E [MPa]	A_{bp} [%]	R_b [MPa]	K_{Ic} [MPa√m]
AB 1	246823	,0.042	2659	16.0
AB 2	235018	0.051	3000	'15.0
PMS	228220	0.052	3247	10.9
PMS A	250000	0.023	27''5	10.3

Tab. 4.3 Mechanical Properties of PM materials
E = Young's modulus, A_{bp} = yield strength in bending
R_b = bending strength, K_{Ic} = fracture toughness

4.3 In-service test

The superior toughness of the double dispersion material encouraged us to test the new material in service. Two die inserts were prepared and shrink-fitted into cold-forging-tools for bolt making. In one series the bolts were cold-forged from annealed wire, in the other series cold-drawn wire of higher strength was used. For reference a standard high-speed steel derived from ingots by hot-roll ng was employed. **To** avoid cracking the reference steel had to be tempered to a much lower hardness as compared to the double dispersion material. As a result, 6 to 8 t me-s more bolts were manufactured with inserts of the new material as compared to the standard steel.

tool No.	die insert * ,	hardness HRC	number of cycles to fracture
1	M 3 class 1	57	9080
2	M 3 class 1	57	10200
3	AB 1	-66	78000

Tab. 4.4 Tool life quantity in bolt making ⌀ 33 x ⌀ 12 x O mm '

5. Summary

A method for the design of, tool materials was developed. In, a first step a particular tooling operation (final heading in bolt making) was numerically simulated in a macroscopical scale. The FEM-model was performed taking into account the internal stresses due to shrink fitting of the. tool and the plastic deformation of the work piece. High stresses were computed in-two regions around the die insert profile radius, These high stressed zones are quit reasonable. In practice, tools often fail due to chipping at these regions. The heading force and the radial and circumferrential strains obtained by FEM-simulation werd compared to experimental results. A close agreement was found.

In a second step the material was modelled on a microscopical scale, again using the

finite element method. The influence of hard phase distribution and orientation on the microcrack initiation and propagation was investigated. Hard phase failure was simulated using a local normal stress criteria, subsequent damage of the matrix by introducing the damage parameter Di. The evolution of failure was found as follows: **First,** single hard phases fail due to cleavage, leading to a redistribution of stresses, which in turn causes neighboring hard phases to fracture. Afterwards plastic bands develop, connecting the individual microcracks. Along these bands damage of the matrix takes place. The matrix network in double dispersion material was found to act as an effective obstacle for microcrack linkage.

In the third step the double dispersion" material was produced by a powder metallurgical production route and tested in the laboratory. Wear resistance and bending strength were comparable to a single dispersion material of the same volume content of hard phases. Fracture toughness was increased about 30 %. In the practical application of bolt making tool's lifetime was increased by a factor of 8.

Acknowledgements

The authors would like to thank the European Union (EU) which sponsered the research activities under contract no.: BRE2.CT92.0150
The Swedish part of this investigation was funded by *National Swedish Agency for Industrial and Technics/ Development, Nutek* (Contract No. 92-04946P), which is gratefully acknowledged.
The authors would, furthermore, like to thank Rolf Carlsson, *Bulten Automotive AB/Sweden*, Max Seitter, *Robert Bosch GmbH/Germany*. Leif Westin, *Erasteel Kloster AB/Sweden and Eberhard Ernst, Krebsöge Sinterholding GmbH/Germany*, for stimulating discussions during the course of the work.

References

[1] Asnafi, N.: "Tool Design in Cold Heading of Fasteners, Part I - Literature Survey and Analytical Modeling", Swedish Institute for Metals Research, IM-3332, Dec. 1995.
[2] Asnafi, N.: "Tool Design in Cold Heading of Fasteners. Part II - Finite Element Simulations and Experimental Analysis", Swedish Institute for Metals Research, IM-3333, March 1996.
[3] Thuvander A. & Schedin E.: "Numerical and Experimental Simulation of Cold Forging of a Collar Hex-Bolt", Swedish Institute for Metals Research, *Report /M-*2867, June 1992.
[4] Westin L.: "Powder metallurgy high-speed steels - a materials course for designers of tools and machine components", Erasteel Kloster AB, Söderfors, Sweden, **p.** 13. See also Product Information on ASP30, Uddeholm Tooling, Sweden.
[5] Product Information on H13 (AISI), Uddeholm Tooling, Sweden.
[6] Private communication with Mr. Rolf Carlsson, Bulten Automotive AB, Sweden. See also *Hårdmetall som verktygs- och konstruktionsmaterial, Sandvik Coromant, Sv-5758*, p. 3 *(in Swedish).*
[7] Private communication with Mr. Rolf Carlsson, Bulten Automotive AB, Sweden
[8] Böhm, H. J., Rammerstorfer, F.G. and Weissenbek E , Comput. Mater. Sci, 1, 117, 1993.

[9] Cornet A. and Lin Guoyu, "Elastisch-plastisches Spannungs-Dehnungsverhalten von zweiphasig hexagonal angeordneter Mikrostruktur", Technical Note GKSS/WMA/95/3, 1995.,

[10] Gross-Weege, A., Weichert, D., and Broeckmann, C. "Finite Element Simulation of crack initiation in' hard two-phase materials", accepted to be published in Comput. Mater. Sci., 1996.

[11] Michel, J. C., in: Proc. of the Int. Seminar on Micromechanics of Materials, (Mecamat 93), Fontainebleau/France, 395, 1993.

[12] Gross-Weege, A., "Numerical investigations of cleavage and decohesion in heterogeneous materials", Diplomarbeit, Line, Bochum, 1992.

[13] Rice, J.R. and Tracey D. M., "On the ductile enlargement of voids in triaxial stress fields", J. Mech. Phys. Solids, 17, 201-217, 1969.

[14] Gunawardena, S. R., Jansson, S. and Leckie, F. A., "Transverse ductility of metal 5atrix composites", in "Failure mechanisms in high temperature composite materials", pp. 23-30, AD-Vol.22/AMD-Vol .122, ASME, NY, 1991.

[15] Broeckmann, C., "Bruch karbidreicher Stable - Experiment und FEM-Simulation unter Berücksichtigung des Gefüges", Dissertation Ruhr-Universität Bochum, s.a. Fortschr.-Ber. VDI, Reihe 18, Nr. 169, Düsseldorf, 1994.

[16] Gross-Weege, A. and Weichert, t)., "FE-Simulation of the damage evolution of particle-reinforced MMCs" Proceedings of the 11th IMF. Galway, September 13-15, 1995.

[17] Berns, H.; Nguyen, v. C.; "A new Microstructure for F M Tooling Materials"; submitted to Metal Physics and Applied Technologies, Krew.